211. Synthesis, Structure, and Redox Chemistry of a Vitamin-B_{12s}-Related Macrocyclic Complex of Cobalt(I)[1])

by **Lorenz Walder***, **Gerhard Rytz**[2]), ***Ulrich Vögeli***[2]), and ***Rolf Scheffold****

Institut für organische Chemie der Universität Bern, Freiestrasse 3, CH-3012 Bern

and **Peter Engel***

Laboratorium für chemische und mineralogische Kristallographie der Universität Bern, Freiestrasse 3, CH-3012 Bern

(13.VIII.84)

Summary

(±)-[1-hydro-8H-HDP]cobalt(I) **1**[3])[4]) is obtained by chemical or electrochemical four-electron reduction of (±)-dibromo- or (±)-dicyano[1-hydroxy-8H-HDP]cobalt(III) **2a** or **2b**[4]), respectively. The crystal and molecular structure of **1** was determined by combination of X-ray analysis and MS, ^{1}H-, and ^{13}C-NMR spectroscopy. Square-planar coordinated Co(I) lies closely to the best plane through the four N-atoms which form the first coordination sphere. Thermodynamic data for the coordination of axial bases with the cation of [1-hydroxy-8H-HDP]cobalt **2** in its different metal oxidation states were determined. The pathway of the overall four-electron reduction of **2a** to **1** was elucidated: it involves a two-electron reduction of the central metal, a two-electron reduction of the macrocycle accompanied by elimination of the OH-group and final protonation at C(1). Evidence for an intramolecular electron transfer between the central metal and the macrocycle is presented.

1. Introduction. – Vitamin B_{12} and a variety of related synthetic Co-complexes are useful catalysts in organic synthesis [3]. Under reducing conditions, the Co-complexes act as electron-transfer reagents and convert electrophilic species (R-X) directly or *via* organometallic intermediates into nucleophilic species ($R^\bullet$ radicals or R^- anions), which undergo further transformations according the reaction conditions. The *actual* species involved in those electron-transfer reactions are Co-(I)-complexes [4].

Co(I)-complexes are extremely reactive, evidence about their structure has, therefore, been acquired but indirectly. In case of vitamin B_{12s}, the ^{1}H-NMR [5] and UV/VIS

[1]) Part 16 on the *Synthesis and Reactions of Porphine-Type Metal Complexes*. Part 15, see [1].

[2]) Present addresses: *G. R., Ciba-Geigy AG*, Forschungszentrum KA, Postfach, 1701 Fribourg; *U. V.* Kantonales Laboratorium, Muesmattstrasse 19, CH-3012 Bern.

[3]) Full name of **1**: [2,2,3,3,7,7,8,8,12,12,13,13,17,17,18,18,-hexadecamethyl-2,3,7,8,12,13,17,18,-octahydro-1*H*,23*H*-10,20-diaza-porphinato]cobalt(*I*); full name of **2a**: dibromo[2,2,3,3,7,7,8,8,12,12,13,13,17,17,18,18-hexadecamethyl-2,3,7,8,12,13,17,18-octahydro-1*H*,21*H*-10,20-diazaporphinato]cobalt(III).

[4]) For the nomenclature of [HDP]-complexes see addendum in [2].

spectra [6], the pK_a [7a] [8], and the constitution [7b] of the protonated complex as well as electrochemical data for the Co(III)/Co(II) couple (B_{12a}/B_{12r}) [9] and the Co(II)/Co(I) couple (B_{12r}/B_{12s}) [10] have been reported. Elemental analysis and spectroscopic data are also published for [tetraphenylporphyrinato]cobalt(I) [11] [12], [tetrasulfophthalocyaninato]cobalt(I) [13], and cobaloxime(I) [14]. Cobaloxime(I) is reported to be protonated in aqueous media at neutral pH [14] [15].

In this paper, we present for the first time the molecular structure of a macarocyclic Co(I)-complex as determined by X-ray and instrumental analysis. The complex **1** *(Scheme 1)* has been chosen as target, because its hydroporphinoid ligand system shows close structural relations to corphin [16] and since the parent Co(III)-complexes **2a,b** are easily synthesized [17]. Like vitamin B_{12a}, the complex **2b** behaves as catalyst in the hydrogenolysis of alkyl halides [18], the reductive elimination [19], and the reductive C,C-bond formation [1] [20] [21]. The mechanism of the reduction of **2a** to the catalytically active Co(I)-compound **1** has been elucidated in detail.

Scheme 1

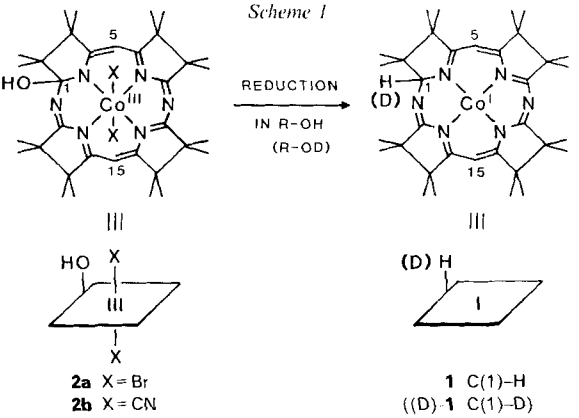

2. Preparation of the Co(I)-complex 1. – Reduction of the red dicyano[1-hydroxy-8H-HDP]cobalt(III) **2b** with $NaBH_4$ in EtOH afforded a dark-green, crystalline compound, $C_{34}H_{51}CoN_6$, in 53% yield. The same compound was obtained in 80% yield by the electrochemical reduction of dibromo[1-hydroxy-8H-HDP]cobalt(III) **2a** at $-1{,}8$ V *vs.* Ag/0.01M $AgNO_3$ in MeOH with consumption of 4 electrons per molecule of **2a**. The extremely O_2-sensitive, diamagnetic compound is soluble in (D_8)THF and shows in its ^{1}H-NMR spectrum the presence of 16 CH_3-groups, 2 *s* corresponding to H–C(5) and H–C(15) at 5.31 and 5.44 ppm as well as one further *s* at 6.38 ppm attributed to H–C(1). Therefore, structure **1** was proposed for the green Co(I)-compound.

Reduction of **2b** with $NaBD_4$ in EtOH gave the same compound **1**, but reduction of **2b** with either $NaBH_4$ or $NaBD_4$ in EtOD afforded in 66 and 53% yield, respectively, the Co(I)-compound (D)-**1**, $C_{34}H_{50}CoDN_6$, whose ^{1}H-NMR spectrum differs from that of **1** only by the absence of the signal at 6.38 ppm. The H or D introduced by the reduction is not acidic. No H,D-exchange was observed in presence of NaOD.

3. Crystal and Molecular Structure of 1. – 3.1. *X-Ray Analysis.* Dark-green, very air-sensitive crystals of **1** ($C_{34}H_{51}CoN_6$, mol. wt. 602.8) of prismatic shape elongated along the unique *b* axis were grown during the reduction of **2a** with $NaBH_4$ (see above). For X-ray investigation, suitable crystals were prepared under N_2 and

coated with a thin film of clear nail polish *(Cutex)*. Preliminary *Weissenberg* photographs with CuK_α-radiation (γ_1 = 1.54051, γ = 1.54433 Å) indicated monoclinic symmetry with systematic absences $h0l$, $l = 2n + 1$, consistent with either space group Pc or $P2/c$. Only reflections up to $\theta = 60°$ could be observed resulting in a rather low resolution of 2 $\sin\theta/\gamma$ = 1.1 Å. Accurate cell parameters were calculated by a least-squares procedure from 16 reflections with $45° < \theta < 60°$ measured on zero-level *Weissenberg* photographs, calibrated with Si-powder lines (a_0 = 5.43088 Å) around the a and b axis. The final lattice parameters are: a = 13.250(8), b = 10.896(8), c = 13.037(9)Å; β = 119.15(5)°; V = 1643.8 Å^3; 2 formula units per unit cell. The calculated density of 1.217 g·cm^{-3} for two formula units is somewhat higher than the experimental density of 1.17(5) g·cm^{-3} measured by flotation in an aqueous NaCl solution under Ar.

Table 1. *Fractional Coordinates and Isotropic Temperature Factors with Standard Deviation for [1-Hydro-8H-HDP]cobalt(I)* **1**

Atom	x	y	z	B
Co	0.500	0.2488(4)	0.350	2.1(2)
N(10)	0.236(2)	0.251(3)	0.336(2)	5.9(7)
N(20)	0.772(2)	0.205(2)	0.407(2)	3.4(7)
N(21)	0.643(2)	0.342(2)	0.430(2)	3.5(7)
N(22)	0.425(2)	0.353(2)	0.415(1)	1.4(6)
N(23)	0.359(2)	0.165(2)	0.266(1)	1.9(6)
N(24)	0.569(2)	0.133(2)	0.296(2)	2.7(7)
C(1)	0.740(2)	0.330(3)	0.417(3)	7.3(8)
C(2)	0.844(2)	0.376(2)	0.544(2)	3.9(7)
C(3)	0.777(2)	0.495(3)	0.535(2)	5.1(7)
C(4)	0.664(2)	0.443(2)	0.491(2)	3.3(7)
C(5)	0.575(2)	0.499(3)	0.518(2)	5.7(7)
C(6)	0.472(2)	0.444(2)	0.502(2)	2.9(7)
C(7)	0.389(2)	0.506(3)	0.528(2)	4.7(7)
C(8)	0.283(2)	0.477(2)	0.426(2)	2.9(7)
C(9)	0.317(1)	0.344(3)	0.398(3)	6.0(8)
C(11)	0.248(2)	0.199(2)	0.249(2)	2.9(7)
C(12)	0.161(2)	0.107(3)	0.188(2)	5.4(7)
C(13)	0.211(2)	0.006(3)	0.157(3)	6.4(8)
C(14)	0.339(2)	0.061(3)	0.191(2)	4.1(7)
C(15)	0.399(2)	0.010(3)	0.157(3)	5.3(8)
C(16)	0.525(2)	0.040(2)	0.229(2)	2.7(7)
C(17)	0.601(2)	− 0.017(3)	0.180(3)	5.3(8)
C(18)	0.726(2)	0.047(3)	0.268(3)	5.0(7)
C(19)	0.692(2)	0.135(3)	0.328(3)	5.4(8)
C(25)	0.885(2)	0.314(4)	0.673(3)	9.0(9)
C(26)	0.952(2)	0.388(3)	0.522(2)	3.8(8)
C(27)	0.771(3)	0.555(4)	0.419(3)	7.6(8)
C(28)	0.828(3)	0.584(3)	0.644(3)	6.0(8)
C(29)	0.399(2)	0.424(4)	0.633(2)	6.7(8)
C(30)	0.423(2)	0.635(3)	0.571(2)	5.7(8)
C(31)	0.227(3)	0.559(4)	0.318(3)	8.0(8)
C(32)	0.187(3)	0.457(4)	0.464(3)	8.1(8)
C(33)	0.065(3)	0.090(4)	0.220(4)	9.2(9)
C(34)	0.116(2)	0.179(4)	0.069(3)	7.5(8)
C(35)	0.237(3)	− 0.094(4)	0.259(3)	7.3(8)
C(36)	0.160(3)	− 0.048(3)	0.027(3)	6.8(8)
C(37)	0.561(3)	0.039(4)	0.049(3)	6.8(9)
C(38)	0.608(2)	− 0.159(3)	0.179(3)	5.5(8)
C(39)	0.825(2)	0.059(3)	0.248(3)	6.4(8)
C(40)	0.752(3)	− 0.067(3)	0.357(3)	7.5(9)

For intensity measurements, a small crystal with approximate dimensions 0.15 × 0.2 × 0.3 mm was used. The intensities were recorded with a *Supper* two-circle diffractometer equipped with a graphite monochromator using Mo$K_{\bar{\alpha}}$-radiation ($\gamma_{K\bar{\alpha}} = 0.71069$ Å). In layers 0–8 around the *a*-axis and layers 0–7 around the *b*-axis, a total of 3444 reflections out to a value of $\theta = 23°$ were recorded at 18°C. Intensities were calculated from the total scan counts (P) and background counts ($B1$, $B2$), measured for $1/m$ of the time of the peak scan, by the relationship $I = P\text{-}m(B1 + B2)$. The intensities were assigned standard deviation according to the formula $\sigma^2(I) = P + m^2(B1 + B2)$. Reflections with $I < 2.57\sigma(I)$ were assumed as unobserved. *Lorentz*-polarization corrections were calculated, but no absorption correction was applied (μMo$K_{\bar{\alpha}} = 5.76$ cm^{-1}). Relative scale factors for each layer were calculated following *Hamilton, Rollett & Sparks* [22] and equivalent reflections were averaged resulting in a total of 2232 unique reflections of which 568 were unobserved. The agreement factor between equivalent reflections is 0.05. The statistical intensity test did not give a clear indication whether the centrosymmetric or noncentrosymmetric space group should be considered. In the centrosymmetric space group *P2/c*, the Co-complex would have to lie on special position on a two-fold axis which is the only possibility compatible with the symmetry of the Co-complex. However, the orientation of the Co-complex as obtained from the *Patterson* synthesis excluded this possibility leaving only the noncentrosymmetric space group *Pc*. The position of the Co-atom was deduced from the *Patterson* synthesis, and a successive *Buerger* minimum function [23] using both Co-positions in the unit cell revealed most atoms of the porphyrin ring. A subsequent *Fourier* synthesis exhibited the complete Co-complex. The refinement was carried out with block-diagonal least-squares routine, the function minimized being $\sum_H w(F_o - \frac{1}{k}F_c)^2$. Atomic scattering factors and anomalous dispersion factors for Co ($\Delta f' = 0.299$, $\Delta f'' = 0.973$) were taken from [24]. Due to the low resolution, the convergence of the least-squares refinement was insufficient, and some of the CH_3-groups had to be constrained to normal C–C bond length. H-atoms were not detected in a difference *Fourier* synthesis and were therefore not included into the refinement. A definitive decision between N- and C-atoms could not be made; therefore, the assignment of N(10) and N(20) is arbitrary. The final agreement factor was $R = 0.103$ for 1664 observed reflections. Fractional coordinates and isotropic temperature factors for the non-H-atoms are given in *Table 1*.

Tables containing bond lengths, bond angles as well as observed and calculated structure factors and selected torsion angles are available as supplementary material. All calculations and drawings were done using the program system *KRIPROG* [25].

The projection of the atomic positions onto the least-squares plane defined by Co and the 4 inner N-atoms in (±)-[1-hydro-8H-HDP]cobalt(I) **1** is shown in *Fig. 1* . Due to the low resolution, the indicated bond lengths are not very accurate, however, the expected pattern of alternating bond lengths in the conjugated system is significant. The interatomic distances are comparable to those in cobalt(III) corrinoids [26] and structurally related porphine-type Ni-complexes [27–29]. A slight non-planarity and

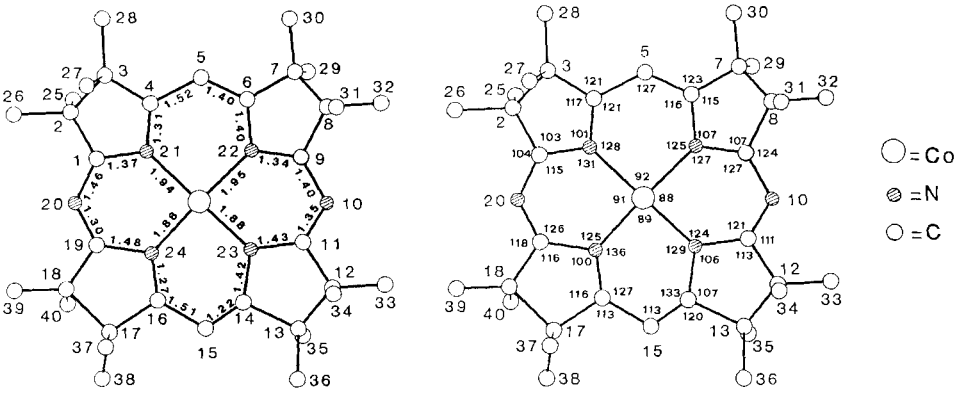

Fig. 1. *Top view of the crystal structure of [1-hydro-8H-HDP]cobalt(I)* **1** including numbering system, selected bond length (left) and selected bond angles (right).

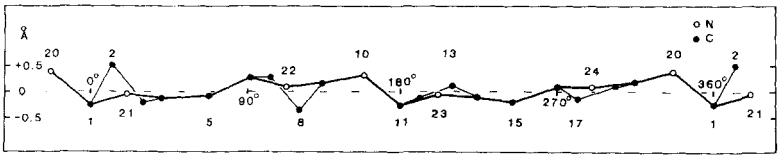

Fig. 2. *Cylindrical projection of* **1** (centre: Co). The vertical displacement of each atom of the macrocycle is referred to the least-squares plane of the four N-atoms N(21) to N(24) and Co. CH_3-groups are omitted for clarity.

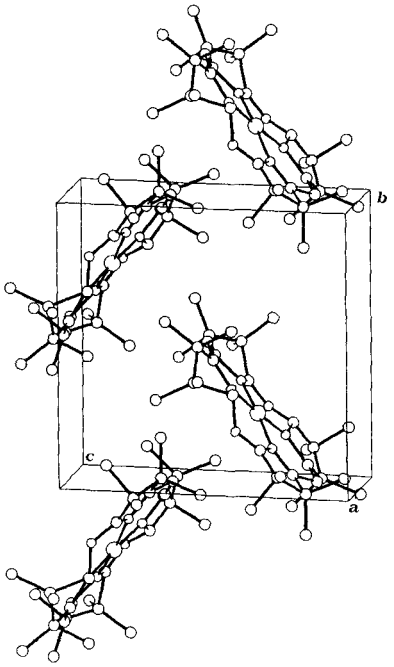

Fig. 3. *Packing diagram for* **1**

saddle-shaped appearance of **1** as emphasized by *Fig. 2* resembles the buckling observed in the corrin ring [26]. The largest deviation of macrocyclic non-H-atoms from the best plane is 0.39 Å (N(20), *Fig. 2*). N(22) and N(24) are placed above, N(21) and N(23) beyond, and the Co is displaced by only 0.025 Å from the best plane. Thus, the 4 inner N-atoms form a very flat tetrahedron with the Co-atom localized in its centre.

For C(1), the mean bond angle to non-H-atoms is 107.5°, close to the tetrahedral angle.

A H-atom at C(1) was detected by NMR spectroscopy as described below. The fact that C(1) and – to a smaller extent – C(11) show pyramidal configuration indicates a nonuniform structural arrangement of identical molecules differing by a 180° rotation about the axis perpendicular to the best plane.

The packing diagram *(Fig. 3)* reveals no close intermolecular contacts, the shortest distances being C(33)...C(39′) = 3.40 Å, Co...C(30″) = 3.50 Å and C(32)...C(26‴) = 3.62 Å. Molecules are hold together by *van der Waals* forces only. No axial ligands and/or solvent molecules were detected.

3.2. *NMR and MS Analysis.* Since the position of the H-atom introduced during the reduction could not be determined by X-ray analysis, additional MS and NMR studies were necessary. Mass spectroscopy and cluster analysis of the M^+ peak clearly

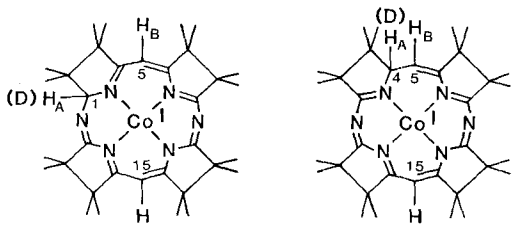

1 ((D)-**1**) **1'** ((D)-**1'**)

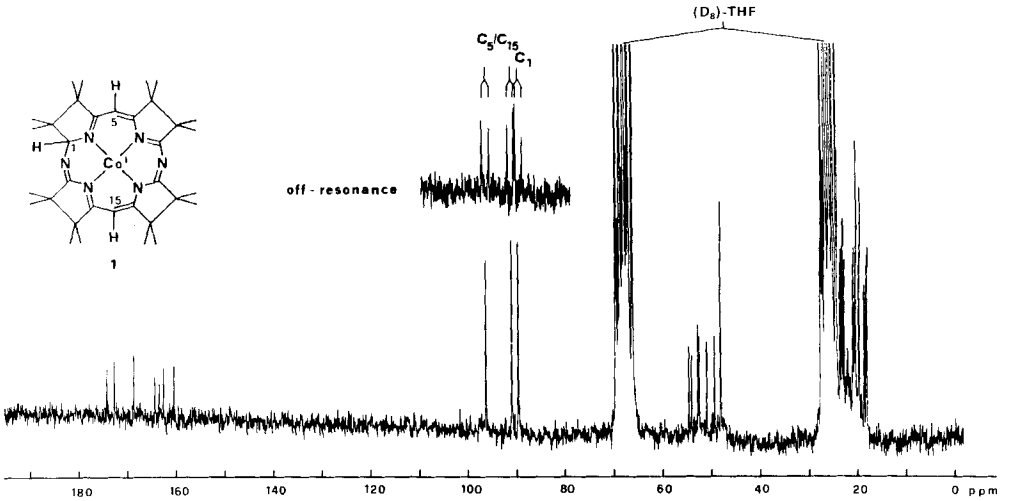

Fig. 4. *^{1}H-noise-decoupled ^{13}C-NMR spectrum ((D_8)THF) of* **1**

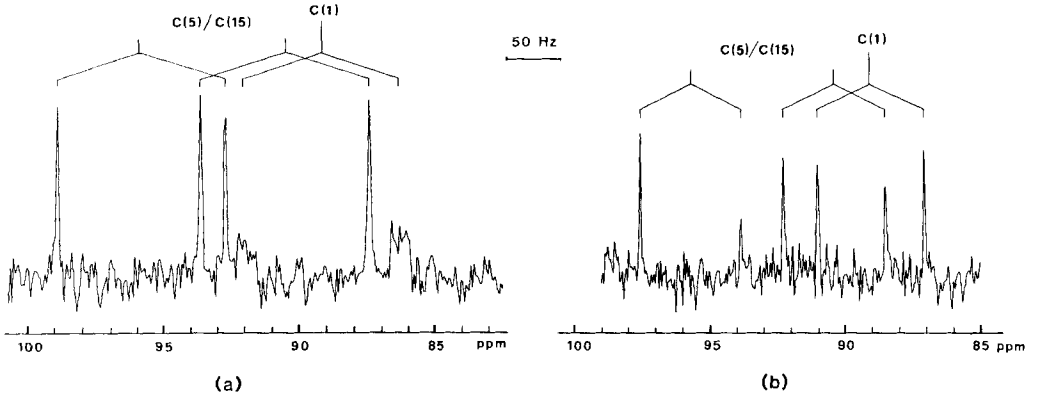

Fig. 5. a) *Non-decoupled ^{13}-C-NMR spectrum of the tertiary C-atom region of* **1**. b) *Same region as* a) *but upon selective irradiation at the centre of the CH_3-resonances (1.19 ppm).*

indicate $C_{34}H_{51}CoN_6$ for **1** or **1'** (structural isomers) and $C_{34}H_{50}CoDN_6$ for (D)-**1** or (D)-**1'**.

From the ^{1}H-NMR spectrum of the diamagnetic reduction product **1**(**1'**), the symmetry group C_1 is deduced (more than 8 lines for the CH_3-groups). The signal at 6.38 ppm, which is absent in the deuterated reduction product (D)-**1** ((D)-**1'**), appears as a *s* with $\Delta\nu_{1/2} = 2$ Hz. These findings are compatible with structure **1** and (D)-**1**, respectively, but do not exclude **1'** and (D)-**1'**, since the vicinal coupling constant between H_A and H_B might be small for a dihedral angle near 90°. However, the specific formation of only one reduction product is confirmed by ^{13}C-NMR spectroscopy *(Fig. 4* and *5)*.

The proton-coupled spectrum *(Fig. 5a))* shows 2 *d* for C(5) and C(15) and 1 *d* of nonresolved *m* (due to coupling to the CH_3-groups) for C(1). Its chemical shift (89.1 ppm in the noise-decoupled spectrum, *Fig. 4*) is typical for a tertiary aminal C-atom as realized in structure **1**. In the case of **1'**, the absorption of C(4) would be expected to lie between 60 and 75 ppm [30].

A strong argument in favour of **1** (and against **1'**) is the fact that C(5) and C(15) give rise to *d*'s without any fine splitting ($\Delta\nu_{1/2} = 2.0$ Hz, *Fig. 5*a)). In **1'**, C(5) would exhibit a geminal C,H coupling with *H*–C(4)[5]). Furthermore, the C(1) signal collapses to a *d* without any fine splitting ($\Delta\nu_{1/2} = 1.5$ Hz) upon irradiation of the CH_3-protons *(Fig. 5b))*. A structure assignment **1'** is furthermore disproved, since for **1'** a splitting due to geminal coupling ($^2J_{C(4),\,H\text{–}C(5)} \approx 3$Hz) [32] is expected. Therefore, the constitution of **1** proves to be right for the Co(I) compound.

4. Electrochemistry of Porphine-Type Co-Complexes. – a) *Electrochemistry in DMA and DMF.* Cyclic voltammograms of **2a** in deaerated *N,N*-dimethylacetamide (DMA) or *N,N*-dimethylformamide (DMF) are shown in *Fig. 6* (see I and II). The

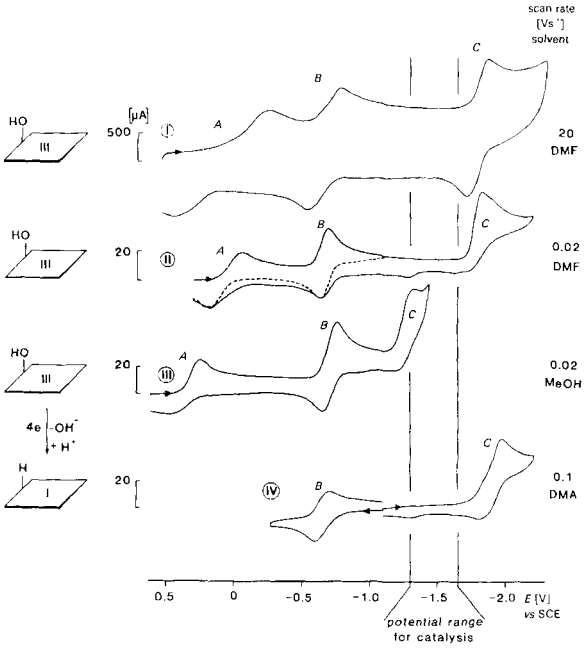

Fig. 6. *Cyclic voltammetry on a glassy carbon electrode at different scan rates of 0.002*M **2a** *(I, II, III), 0.001*M **1** *(IV) in DMA (0.09*M *Bu_4NClO_4, 0.01*M *Bu_4NBr; IV), in DMF (0.09*M *Et_4NClO_4, 0.01*M *Et_4NBr; I, II,) and in MeOH (0.09*M *$LiClO_4$, 0.01*M *LiBr; III)*. Axial coordination omitted.

[5]) This interaction is expected to be somewhat smaller than the typical value of 6–7 Hz for C_{sp2}–C_{sp3}–*H* [31], due to the influence of the N-atom as an electronegative substituent. This is in agreement with our experimental value $^2J_{H,C} = 5.0 \pm 0.2$ Hz for the interaction between H at the benzylic C-atom and the adjacent aromatic C in *N*-benzylformamide.

Co(III)-complex undergoes 3 redox processes. Equal cathodic and anodic peak currents ($i_{pc} \approx i_{pa}$) are also observed for wave *C* at scan rates $\geqslant 5$ Vs^{-1}. Peak potential separation (ΔE_p) within wave *A* is large ($\Delta E_p \approx 200$ to 400 mV, even at low scan rates and depending on [Br^-]), wave *B* exhibits an almost *Nernstian* behaviour at low scan rate ($\Delta E_p \approx 70$ to 90 mV depending on [Br^-])[6]).

Coulometric measurements obtained from an electrolysis in DMA or DMF on the plateau of the first wave show one electron being involved in redox couple *A*. Equal formal potentials $E^{o'}$ are observed by cyclic voltammetry for **2a** and after one-electron bulk reduction of **2a**. Electrolysis of **2a** in DMA or DMF on the plateau of wave *B* indicates one electron being involved in redox process *B*. A more detailed study of i_{pc} as a function of (scan rate)$^{1/2}$ ($= v^{1/2}$) is shown in *Fig. 7*. The i_{pc} of wave *A* and *B* increase linearly up to 1 Vs^{-1}. The different slopes *A* and *B* are due to the slow electron-transfer rate of redox process *A* and, at slow scan rates, to the electrochemically reversible nature of wave *B* consistent with the observed ΔE_p[7]). The i_{pc} of wave *C* approaches slope *B* at high scan rates, whereas at slow scan rates, the slope of the limiting straight line *C* indicates a two-electron process (slope *C*/slope *B* = 2.1).

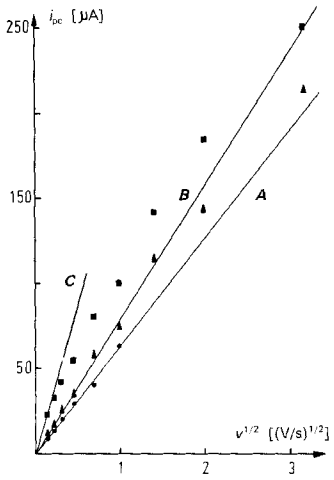

Fig. 7. *Cathodic peak currents* (i_{pc}) *of cyclic voltammograms of* **2a** *(0.001 M) in DMF (0.49 M Bu_4NClO_4, 0.01 M Bu_4NBr)* vs. *(scan rate)*$^{1/2}$ *($= v^{1/2}$)*

The three oxidoreduction reactions may be attributed to either metal- and/or macrocyclic-ligand-localized reactions. If a change in oxidation state is accompanied with a change of the affinity of the central metal towards axial ligands, it may be concluded, that an orbital with substantial metal character is populated by the extra electron. In order to elucidate the metal and/or ligand character of wave *A*, *B* and *C* extensive studies of $E^{o'}$(*A*, *B*, and *C*) in presence of different amounts of free axial ligand have been performed[8]). $E^{o'}$(*A*, *B*, and *C*) have been calculated either from the average of cathodic and anodic peak potentials (E_{pc}, E_{pa}) of cyclic voltammograms at slow scan

[6]) The electron-transfer rate of redox process *A* has been found to be drastically enhanced by addition of Br^-, whereas redox process *B* is slowed down at higher [Br^-].

[7]) According to $i_{p,rev.} = FAC^{\circ} \cdot D^{1/2} \cdot (F/RT)^{1/2} \cdot V^{1/2}$ and $i_{p,irrev.} = 0.496 \cdot \alpha^{1/2} \cdot FAC^{\circ} \cdot D^{1/2} (F/RT)^{1/2} \cdot V^{1/2}$, the observed ratio of slope *B*/slope *A* = 1.16 agrees with theory, if the transfer coefficient for the redox process *A* is 0.6.

[8]) Similar studies have been presented by *Kadish* [33] and *Davis* [34] for porphyrinatocobalts.

rate (20 mVs^{-1}) or from the average peak potential of slow positive and negative scans of differential pulse voltammetry. Both techniques insure that ligand-exchange kinetics do not interfere with $E^{o'}$. Results obtained from cyclic voltammetry are consistent with those from differential pulse voltammetry. Redox process *C* exhibiting chemical irreversibility at slow scan rates has been studied with cyclic voltammetry at 1 Vs^{-1}. Changes in the axial coordination number ($(p-q)$ or q) due to changes of the metal oxidation state were determined by the slope of the formal potential $E^{o'}$ as a function of log(ligand concentration) (log[L]) from *Eqn. 1* and *2*.

$$E_L^{o'(III/II)} - E_S^{o'(III/II)} = -0.059 \cdot V \cdot \log\frac{K^{III}}{K^{II}} - 0.059 \cdot V \cdot (p-q) \cdot \log[L] \quad (1)$$

$$E_L^{o'(II/I)} - E_S^{o'(II/I)} = -0.059 \cdot V \cdot \log K^{II} - 0.059 \cdot V \cdot q \cdot \log[L] \quad (2)$$

$E_S^{o'}$ is the formal potential in pure solvent/electrolyte. K^{III}, K^{II}, p, and q are defined by *Eqn. 3* and *4*.

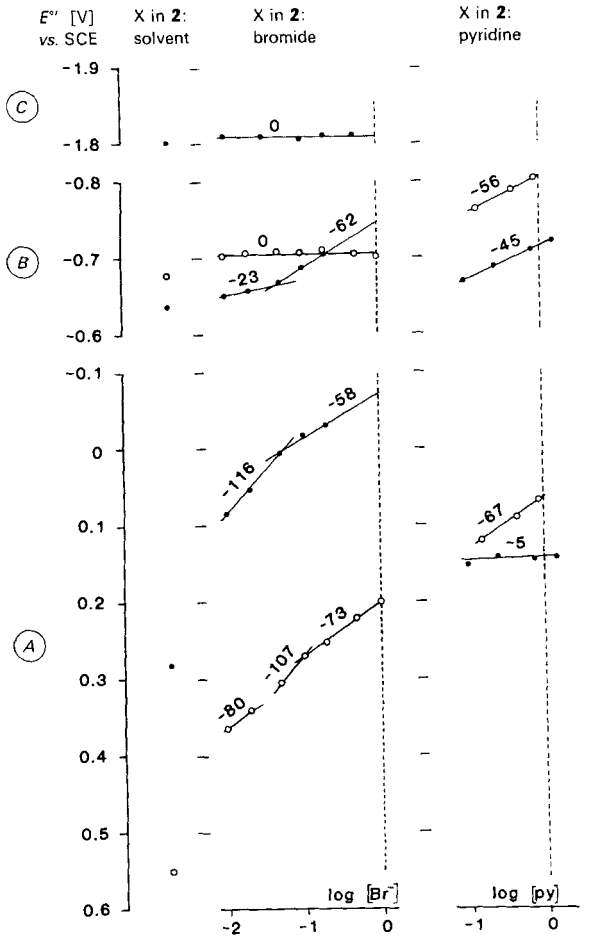

Fig. 8. *Formal potentials ($E^{o'}$) of* **2** *(0.001 M) in MeOH* (o), *DMA or DMF* (●) vs. *SCE*. $E^{o'}$ (*A*, *B*, and *C*) in pure solvent/0.1 M $LiClO_4$ or Et_4NClO_4 at increasing $[Br^-]$ ($[ClO_4^-] + [Br^-] = const.$) and at increasing [py]. $E^{o'}$ (*A* and *B*) from cyclic voltammetry at 0.02 Vs^{-1}, $E^{o'}(C)$ at 1 Vs^{-1} on a glassy carbon electrode.

$$Co^{III}\cdot S_x + p\cdot L \; K^{III} \rightleftarrows Co^{III}\cdot L_p + x\cdot S \quad (3)$$

$$Co^{II}\cdot S_y + q\cdot L \; K^{II} \rightleftarrows Co^{II}\cdot Lq + y\cdot S \quad (4)$$

Assuming that Co(I) is not coordinated by axial ligands *Eqn. 2* yields q (the number of L axially bound to Co(II)) and K^{II}[9]). Thence p (the number of axially coordinated L on Co(III)) and K^{III} can be calculated from *Eqn. 1*.

Plots of $E_L^{o'}$ *vs.* log[L] (L = Br^- or pyridine) in DMA or DMF as well as $E_S^{o'}$ of the ligand-free complex are shown in *Fig. 8*. Approximate multiples of −59 mV are found for the slopes of $E_L^{o'}(A)$ and $E_L^{o'}(B)$ in DMA as a function of log[Br^-], whereas no dependence of $E^{o'}$(C) on axial-ligand concentration is observed. Wave *A* and *B* in DMA or DMF have, therefore, to be assigned to two metal-reduction processes accompanied with loss of one Br^- at [Br^-] = 1M, whereas wave *C* (in DMF) is due to a macrocyclic-ligand reduction (according to equilibria *A1*), *B1*) and *C1*), resp., in *Table 2*). The same measurements have been carried out with pyridine as axial ligand. Results are reported in *Fig. 8*. The slopes of −5 and −45 mV for $E^{o'}(A)$ and $E^{o'}(B)$ (in DMA), respectively, have been interpreted as one pyridine being bound to Co(III) but only released on wave *B* upon reduction to Co(I) according to equilibria *A3*) and *B3*) in *Table 2*. $E_L^{o'}$-values extrapolated to [L] = 1M and $E_S^{o'}$ in pure DMA/supporting electrolyte have been used to calculate K^{III} and K^{II} (*Table 3*).

Table 2. *Selected Formal Potentials*

Electrode reaction at [L] = 1M			$[V]^{E^{o'}}_{vs.\ SCE}$	Solvent
A				
1) Co(III)(R–OH^-)Br_2[a])	+ e^-⇄Co(II)(R–OH^-)Br	+ Br^-	− 0.075	DMA
2) Co(III)(R–OH^-)Br_2	+ e^-⇄Co(II)(R–OH^-)Br	+ Br^-	+ 0.200	MeOH
3) Co(III)(R–OH^-)pyS]$^{2+}$	+ e^-⇄Co(II)(R–OH^-)py]$^+$ + S			
	or Co(II)(R–OH^-)pyS]$^+$		+ 0.140	DMA
4) Co(III)(R–OH^-)py_2]$^{2+}$	+ e^-⇄Co(II)(R–OH^-)py]$^+$	+ py	+ 0.065	MeOH
5) Co(III)(R–OH^-)DMA_x]$^{2+}$	+ e^-⇄Co(II)(R–OH^-)DMA_y]$^+$		+ 0.280	DMA
6) Co(III)(R–OH^-)$MeOH_x$]$^{2+}$	+ e^-⇄Co(II)(R–OH^-)$MeOH_y$]$^+$		+ 0.550	MeOH
B				
1) Co(II)(R–OH^-)Br	+ e^-⇄Co(I)(R–OH^-)	+ Br^-	− 0.750	DMA
2) Co(II)(R–OH^-)Br	+ $2e^-$⇄Co(I)(R$^{\cdot-}$)[b])	+ Br^- + OH^-	− 0.700	MeOH
3) Co(II)(R–OH^-)py]$^+$	+ e^-⇄Co(I)(R–OH^-)	+ py	− 0.715	DMA
4) Co(II)(R–OH^-)py]$^+$	+ $2e^-$⇄Co(I)(R$^{\cdot-}$)	+ py + OH^-	− 0.805	MeOH
5) Co(II)(R–OH^-)DMA_x]$^+$	+ e^-⇄Co(I)(R–OH^-)		− 0.640	DMA
6) Co(II)(R–OH^-)$MeOH_x$]$^+$	+ $2e^-$⇄Co(I)(R$^{\cdot-}$)	+ OH^-	− 0.675	MeOH
C				
1) (Co(I)(R–OH^-)	+ e^-⇄Co(I)(R–$OH^{2\cdot-}$)[c])		− 1.81	DMF

[a]) (R–OH^-) corresponds to the macrocyclic ring in **2**, **3**, and **4** in *Scheme 2*.
[b]) (R$^{\cdot-}$) corresponds to either macrocyclic ring in **9** or **12** in *Scheme 2*.
[c]) (R–$OH^{2\cdot-}$) corresponds to the macrocyclic ring in **5** in *Scheme 2*.

[9]) This assumption is consistent with the X-ray structure of **1**. Other Co(I) macrocyclic compounds show no axial coordination *e.g.* vitamine B_{12s} [10], [tetraphenylporphyrinato]cobalt(I) [33].

Table 3. *Stability Constants for Complexation of [1-Hydroxy-8H-HDP]cobalt(III) and -cobalt(II) by Pyridine and Br⁻*

Solvent	$\log K^{II}$		$\log K^{III}/K^{II}$		$\log K^{III}$	
	py	Br^-	py	Br^-	py	Br^-
MeOH	2.2 ± 0.2 [a] [e]	$\approx 1.0 \pm 0.3$ [a] [e]	8.3 ± 0.2	6.6 ± 0.2	10.5 ± 0.4 [b] [e]	6.6 ± 0.2 [b] [e] 1.6 ± 0.2 [c] [f]
DMA	1.3 ± 0.2 [a]	1.9 ± 0.1 [a]	2.4 ± 0.2	6.1 ± 0.2	3.7 ± 0.3 [d]	8.0 ± 0.3 [b]

[a] $Co^{II} \cdot S + L \overset{K}{\rightleftarrows} Co^{II} \cdot L + S$ (S = solvent).
[b] $Co^{III} \cdot S + 2L \overset{\beta}{\rightleftarrows} Co^{III} \cdot L_2 + S$.
[c] $Co^{III} \cdot L \cdot S + L \overset{K2}{\rightleftarrows} Co^{III} \cdot L_2 + S$.
[d] $Co^{III} \cdot S + L \overset{K1}{\rightleftarrows} Co^{III} \cdot L + S$.
[e] May be influenced by loss of OH^- on the macrocycle.
[f] Determined by UV spectroscopy.

We reported earlier about the reversible acid-induced elimination of OH^- from the macrocycle of **2** leading to the [16]annulene ligand system according to equilibrium **2⇆6** in *Scheme 2* [17]. The observed peak-current behaviour of the ligand wave *C* going from a reversible one-electron reduction at fast scan rates to an irreversible two-electron reduction at slow scan rates may, therefore, be interpreted as a reductively induced elimination of OH^- yielding a radical anion on the macrocycle which takes up another electron at the same potential and undergoes irreversible chemical follow-up reactions.

Scheme 2

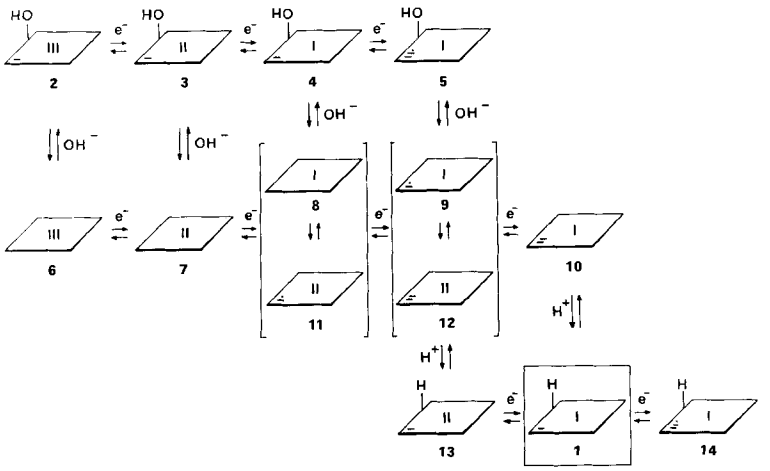

b) *Electrochemistry in MeOH.* A cyclic voltammogram of **2a** in MeOH is shown in *Fig. 6 (see III)*. Again, three waves *A*, *B*, and *C* can be distinguished. Approximately equal cathodic and anodic peak currents are observed within couple *A* and *B* if the scan direction is reversed between couple *B* and *C*. Wave *C* which is located in the foot of the cathodic solvent reduction shows no anodic current, even at 50 Vs^{-1}. Peak potential separation of wave *A* is large (90 to 220 mV, even at slow scan rate and depending on [L]). ΔE_p of wave *B* in MeOH indicates a slower electron transfer than in DMA ($\Delta E_p \approx 100$ to 150 mV depending on scan rate and [L])[6]. Bulk electrolysis on the

plateau of the first wave reveals that one electron is involved in redox couple *A*. Electrolysis of **2a** on a mercury-pool electrode potentiostated on wave *C* consumes approximately 4 electrons per **2a** and yields **1**. Coulometry conducted on the plateau of wave *B* is not conclusive. The i_{pc} of wave *A* is increasing linearly with (scan rate)$^{1/2}$ up to 50 Vs^{-1} whereas i_{pc} of redox couple *B* behaves nonlinearly approaching slope *A* at high scan rates *(Fig. 9)*. At slow scan rates, a limiting straight line with a remarkable ratio of the two slopes is observed, *i.e.* slop *B*/slope *A* = 2. To the same extent as the slope of $i_{pc}(B)$ is approaching slope *A*, the third wave *C* diminishes. If the glassy carbon electrode is equilibrated for several seconds on wave *B* and scanned with 50 Vs^{-1} in negative direction, wave *C* is fully developed. We may, therefore, conclude that wave *B* corresponds to a two-electron reduction at slow scan rates yielding an electroactive product indicated by wave *C*.

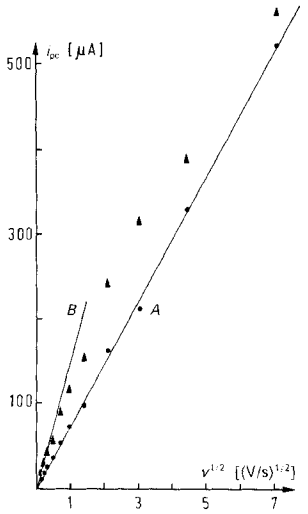

Fig. 9. *Cathodic peak currents (i_{pc}) of cyclic voltammograms of* **2a** *(0.001 M) in MeOH (0.09 M $LiClO_4$, 0.01 M LiBr)* vs. *(scan rate)$^{1/2}$ ($= v^{1/2}$)*

In DMF, a reversible one-electron reduction of the macrocycle was found at −1.81 V *vs.* SCE. At slow scan rates, a two-electron reduction was observed at the same potential. These results were interpreted by an ECE mechanism, C corresponding to loss of OH^-. In the protic solvent MeOH, loss of OH^- from the macrocycle is favoured and occurs at slow scan rate already on wave *B* giving rise to the [16]annulene ligand system which takes up another electron at the same potential. If the scan is reversed between wave *B* and *C* this compound is reoxidized and attacked by OH^- or methanolate according to the pathway **3**→**4**→**8**/**11**→**9**/**12**→**8**/**11**→**7**→**3** in *Scheme 2*. Consistent with the proposed mechanism is the fact that multiple cyclic-voltammetry scans on wave *B* do not differ significantly from a single scan.

Redox couple *A* and *B* have been assigned to metal- and/or macrocyclic-ligand reduction based on the criterion of $E^{o'}$ dependence on axial ligand concentration. Approximate slopes of −59 mV in slow-scanning cyclic voltammetry for **2** in MeOH for increasing log[py] are observed, indicating loss of one pyridine in each redox couple *A* and *B* at [py] = 1 M *(Fig. 8;* equilibria *A4)*, *B4)* in *Table 2)*. K^{III} and K^{II} values are

reported in *Table 3*[10]). The dependence of $E^{o'}(A)$ and $E^{o'}(B)$ on growing $[Br^-]$ is more complicated. Dissociation of 1 Br^- from **2a** is observed upon dissolution of **2a** in MeOH/$LiClO_4$. The stability constant for the equilibrium $Br^- + [\mathbf{2a}\text{–}Br^+] \rightarrow \mathbf{2a}$ is *ca.* 40 as determined by UV spectroscopy[11]). In agreement with these results, a change of the slope from −80 to −107 mV occurs for wave *A* of **2a** in MeOH at $\log[Br^-] \approx -1.6$ *(Fig. 8)*. Another change of the gradient from −107 to −73 mV is observed at $\log[Br^-] \approx 1$, suggesting that **2a** is reduced with concomitant loss of 1 Br^- at $[Br^-] \approx 1$. Anyhow, $E^{o'}$ of wave *B* doesn't show any dependence on bromide concentration at $[Br^-] = 1$. Either kinetics of the OH^- loss from the macrocycle determine $E_{1/2}(B)$ or the central metal is still in its oxidation state II after reduction implying that **12** dominates the equilibrium **9**⇄**12** (Scheme 2). Additional evidence for the proposed reduction and reoxidation mechanism of **2a** on wave *B* is shown in *Fig. 10*. At fast scan rate, one-electron reduction takes place according to i_{pc} *vs.* (scan rate)$^{1/2}$ in *Fig. 9*. A single anodic wave at peak potential *M* is observed. At intermediate scan rates, partly one- and partly two-electron reduction occurs (wave II and III in *Fig. 10*). At these scan rates, an additional reoxidation wave shows up with a *ca.* 200 mV more positive peak potential *L*. At 20 mVs^{-1} (wave I in *Fig. 10*), a clean two-electron reduction occurs, but the

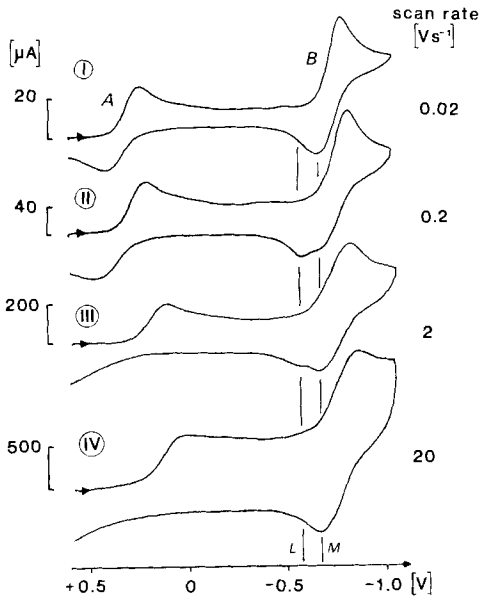

Fig. 10. *Cyclic voltammograms of* **2a** *(0.002M) in MeOH (0.01M LiBr, 0.09M $LiClO_4$) at different scan rates*

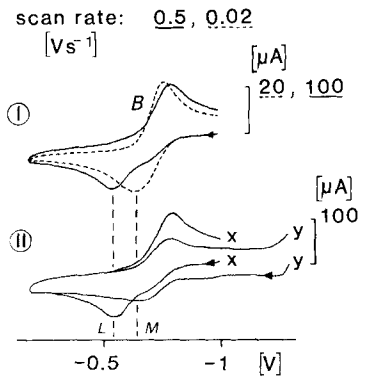

Fig. 11. *Cyclic voltammograms of* **12** *(0.002M; see I and IIx) and* **1** *(0.002M; see IIy) in MeOH (0.09M $LiClO_4$, 0.01 LiBr)*. After bulk electrolysis of **2a** at a Hg-pool electrode at − 1 V consuming $3e^-$ per **2a**. I: at different scan rates. II: starting the sweep at − 1 V (IIx) and at − 1.3 V (IIy).

[10]) $E^{o'}$ measurements of **2** in pure solvent/electrolyte show that DMA stabilizes the Co(III) oxidation state relative to the Co(II) oxidation state to a greater extent than MeOH owing to the different affinity of the two solvents towards Co(III) in accordance to their different *Gutmann Donor Number* [35]. Stability constants of **2** with pyridine or bromide reported in *Table 3* depend, therefore, not only on the inherent affinity of these axial ligands towards Co(III), but also strongly on the solvent ability to interact competitively with Co(III) as well as the solvation of pyridine or bromide by either of the two solvents.

[11]) Isosbestic behaviour for **2a** was observed by UV spectroscopy in MeOH between 300 and 220 nm in presence of increasing amounts of LiBr.

reoxidation wave appears at peak potential *M*. If a solution of **2** is electrolized on the plateau of wave *B*, the two-electron reduction product **9**/**12** may be analized by cyclic voltammetry at different scan rates without affecting its formation. At slow scan rates, oxidation on the metal peak potential (*M*) is possible, but at scan rates ≥ 100 mVs^{-1} oxidation on the ligand peak potential (*L*) is observed (see I in *Fig. 11*). These results indicate that **2a** reduced by 3 electrons overall is a Co(II)-complex with 2 electrons on the macrocycle (**12** in *Scheme 2*). At a high sweep rate, the ring is oxidized and attacked by OH^- or methanolate according to **12**→**11**→**7**→**3**, whereas at slow sweep rate, the equilibrium **9**⇄**12** supplies the Co(I)-compound which is oxidized at the more negative potential *M* according to (**12**→**9**)→(**11**→**8**)→**7**→**3**.

Fig. 11 (see II) shows two cyclic voltammograms. Scans were started once at −1 V (IIx) and once after potentiostating the electrode for some seconds on wave *C* (IIy). In case x, a two-electron oxidation on the ligand potential is observed. In case y, a one-electron oxidation on the metal wave occurs. As by electrolysis of **2a** on wave *C* **1** is formed, we may interprete the cyclic voltammogram IIy *(Fig. 11)* according to **1**→**13**→**1**, **1** being formed during equilibration on wave *C* following the sequence **12**→**10**→**1**. It is interesting to note that protonation of the macrocycle (**10**→**1**) renders metal oxidation possible again. Deprotonation of **13** (**13**→**12**) seems to be negligible on the time scale of cyclic voltammetry.

c) *Electrochemistry of* **1**. Crystalline **1** was dissolved in carefully deaerated DMA/supporting electrolyte yielding a dark-green solution which has been analyzed by cyclic voltammetry (*Fig. 6* see IV). Wave *B* and *C* were observed, but wave *A* was not well defined. Formal potentials $E^{o'}(B)$ and $E^{o'}(C)$ are similar to those of **2a** at the same [Br^-]. $E^{o'}(B)$ *vs.* log[Br^-] shows an approximate −59 mV slope indicating metal character for redox couple *B* (equilibrium **1**⇄**13** in *Scheme 2*). Wave *C* is not affected by growing [Br^-] and may therefore be attributed to a further macrocyclic-ligand reduction according to equilibrium **1**⇄**14** in *Scheme 2*.

d) *Electrochemical and Chemical Synthesis of* **1**. The electrochemical reduction of **2a** in MeOH and the chemical reduction of **2b** with $NaBH_4$ in EtOH led both to [1-hydro-8H-HDP]Co(I) **1**. The formation of **1** with $NaBD_4$ in EtOH and (D)**1** with $NaBH_4$ in EtOD shows clearly that −OH in **2b** is not substituted by a hydride originating from the reducing agent, but the macrocycle is protonated by the solvent. The chemical reduction seems to follow the same pathway as proposed for the electrochemical reduction: Formation of a Co(I)-complex followed by reductive elimination of OH^-, further reduction and protonation at C(1)[12]).

5. Conclusion. – Complex-formation constants of the [1-hydroxy-8H-HDP]Co cation in its different oxidation states with axial bases *(Table 3)* are of the same order of magnitude as those of other catalytically active macrocyclic Co-complexes[13]).

---

[12]) Quenching a solution of **2b** in an early state of $NaBH_4$ reduction with methyl iodide yielded the methylated Co(III)-complex bearing OH on the macrocycle. This result is consistent with the proposed mechanism, *i.e.* protonation being the last step of the sequence (unpublished results).

[13]) Stability constants for pyridine complexation of [tetraphenylporphyrinato]cobalts (= CoTPP) have been reported: logβ values for Co(III)TPP range from 6 to 16 (depending strongly on the solvent), whereas log$K$ values for Co(II)TPP lie between 1.1 and 2.6 [33] [34] [36] [37]. For the intramolecular coordination of the benzimidazole side chain of vitamin B_{12} in H_2O at pH 4.7, log K(III) = 7.1 and log K(II) = 1.8 have been reported [9] [10].

To our knowledge there exists no evidence that macrocyclic Co(I)-complexes coordinates donor ligands in axial positions[14]). This study adds a further proof to this general view. The trend of decreasing stability constants towards axially coordinate ligands in the order Co(III)→Co(II)→Co(I) may be described qualitatively by a three-center 4→5→6 electron-bonding model which combines axial-ligand σ-orbitals with symmetric metal orbitals of substantial d_{z^2} character [37].

Another common feature of efficient catalysts is their macrocyclic π-system. It represents by itself an electroactive subunit. The reduction of the macrocycle occurs generally at 0.5 to 1.1 V more negative potentials than the corresponding Co(II)/Co(I) metal reduction. This difference in reduction potentials prevents electron density at Co(I) to be delocalized into the macrocyclic ligand system; it causes the complex to exhibit metal nucleophilicity.

In this work we have shown that ring reduction may interfere with the Co(II)/Co(I) couple. In protic solvents, the Co(I) complex **4** *(Scheme 2)* loses the OH^- substituent on the macrocycle effecting the reduction potential to shift positively into the Co(II)/Co(I) wave. We have ascribed the product of this reduction to a Co(II) species with two negative charges on the macrocycle (**12**)[15]). Its reoxidation has been found to occur either by direct ligand oxidation or by metal oxidation through equilibrium **12**⇄**9** involving a sluggish intramolecular electron transfer. If **12** is reduced by a further electron (**9**/**12**⇄**10**), protonation of the macrocycle takes place (**10**→**1**). The product **1** of the overall four-electron reduction shows clean metal redox properties on the Co(I)/Co(II) wave on the time scale of cyclic voltammetry and exhibits again a macrocyclic-ligand reduction which is shifted negatively as expected for the interrupted π-system.

We may, therefore, assume that **4** is acting as a catalyst in aprotic solvents, whereas **1** is the efficient catalyst in protic solvents. Reaction **4**→**1** enables the catalyst to preserve its activity by selfadaption to its environment under protic reducing conditions[16]).

This work was supported by the *Swiss National Science Foundation*. We thank Professor *J.M. Savéant* (Paris) for helpful discussions. *G.R.* thanks the *Ciba-Geigy AG* (Basel, Switzerland) for financial support.

Experimental Part

General. All reactions were carried out under Ar using *Schenk* glassware [42]. Solvents (reagent-grade; *N,N*-dimethylacetamide = DMA, *N,N*-dimethylformamide = DMF) were deaerated by bubbling with Ar. EtOD (96% in D_2O, 99,5% D; *Chemische Fabrik Uetikon* CH) was used in the synthesis of (D)-**1**. $NaBH_4$ and $NaBD_4$ (>98% D) were from *Fluka (purum)*. Supporting electrolytes (tetrabutylammonium bromide = Bu_4NBr, tetrabutylammonium perchlorate = Bu_4NClO_4, tetraethylammonium bromide = Et_4NBr, tetraethylammonium perchlorate = Et_4NClO_4) were reagent-grade and twice recrystallized. Spectra were recorded as described [17] and/or: IR as CsI disks on a *Perkin-Elmer* (model *580*), ^{1}H-NMR (80 MHz) on a *Bruker WP 80* spectrometer in

[14]) The X-ray structure of a carbon monoxide stabilized macrocyclic Co(I)-complex has been reported [38]. Anyhow, substantial transfer of electron density from the central atom into the π-acceptor ligand may have taken place in this compound.

[15]) *Busch* [39] as well as *Hush* [40] have reported that other macrocyclic Co-complexes undergo similar intramolecular electron-transfer reactions.

[16]) It is interesting to note that the macrocycle of [didehydrocorrinato]cobalt, a hypothetical biochemical precursor of natural corrins, is reduced by Zn under mild acidic conditions to the corrinatocobalt system [41].

(D_8)THF and with TMS (= 0 ppm) as internal standard. The same solvent was used for ^{13}C-NMR, where C(β) of the solvent with δ_C = 25.2 ppm relative to δ_C = O was used as internal standard. NMR tubes (12 mm) with saturated solutions of **1** and (D)-**1** were sealed under Ar after addition of traces of $NaBH_4$ and $NaBD_4$, respectively.

Electrochemical Apparatus and Procedure. Cyclic voltammetry (CV) and preparative-scale electrolysis were conducted with a *PAR* (model *173/179*) potentiostat/coulometer, a *Tacussel* (model *GSATP*) programmer and a *Philips* (model *PM 8041*) x-y recorder or a *Tektronix* storage oscilloscope, using conventional cells. Differential-pulse voltammograms (DPV) were measured with a *Polarecord E 506 (Metrohm)*. A glassy carbon electrode *(Metrohm EA 276/2)* of 4.8 mm diameter was used for CV and DPV. Electrochemical measurements were obtained at r.t. (21 ± 2°) in solutions deaerated by bubbling with Ar. Potentials were measured with respect to a Ag/0.01M $AgNO_3$ electrode or a KCl-saturated calomel electrode (SCE). In order to reduce a large change in the junction potential during measurements of $E^{o'}$ *vs.* log[Br^-], the total salt concentration was kept constant according to the cell arrangement: SCE/DMA c[Bu_4NClO_4]/DMA x [Bu_4NBr]/y [Bu_4NClO_4] with $x + y = c$. This arrangement insures negligible contamination of the reference electrode by Br^- but doesn't exclude a slightly shifting junction potential (E_j) due to different equivalent conductivities $\lambda_{Bu_4NClO_4}$ and λ_{Bu_4NBr} in DMA. According to the *Lewis-Sargent* equation $E_j = 0.059 \cdot \log(\lambda_{Bu_4NBr}/\lambda_{Bu_4NClO_4})$, the measured formal potentials could be influenced by $\leqslant$ 18 mV if the two λ differ by a factor $\leqslant$ 2. In a control experiment, the formal potential of the nitrobenzene/nitrobenzene $\dot{-}$ redox couple differed only by 8 mV in DMA/0.2M Bu_4NBr and DMA/0.19M Bu_4NClO_4 + 0.01M Bu_4NBr.

Preparation of the Co(1)- complexes **1** *and* (D)-**1**. *[1-Hydro-8H-HDP]cobalt(I)* **1**. The lower compartment of a 100-ml *Schlenk* funnel was completely filled with a solution of 10 mg (0.27 mmol) of $NaBH_4$ in 24 ml of abs. EtOH. To the upper compartment, containing a solution of 20 mg (0.53 mmol) of $NaBH_4$ in 6 ml of abs. EtOH (pH 9), a red solution of 134 mg (0.2 mmol) of dicyano[1-hydroxy-8H-HDP]cobalt(III) **2b** [17] in 1 ml of abs. EtOH was added. The colour changed to deep-green, and crystallization was observed. After 48 h standing at r.t., the crystals were filtered off, washed with 10 ml of EtOH/H_2O 1:1 and 10 ml of H_2O, and dried at 80° (72 h/0.01 Torr): 65 mg (54%) of dark-green **1**. UV (MeOH): 722 (3.32), 616 (3.29), 508 (3.44, sh), 468 (3.57), 370 (4.01). IR: 2970, 1728, 1378, 1134. ^{1}H-NMR: 0.92–1.46 (48H, 16 CH_3 resolved in 10 lines at 0.92, 0.99, 1.01, 1.13, 1.16, 1.27, 1.34, 1.37, 1.40, 1.46); 5.31 (*s*, 1H, H–C(5) or H–C(15)); 5.44 (*s*, 1H, H–C(5) or H–C(15)); 6.38 (*s*, 1H, H–C(1)). No other signals were detected between + 18 and – 27 ppm. Addition of NaOD caused no change of the spectrum. ^{13}C-NMR: 17.3, 17.4, 17.8, 18.9, 19.7, 20.7, 22.0, 22.4, 22.4, 22.8, 23.6, 26.6 (12 CH_3, 4 signals covered by solvent signals); 47.6, 47.6, 48.9, 50.4, 52.0, 52.2, 53.6, 54.1 (8 quart. sp^3–C); 89.1 ($^1J_{C,H}$ = 145, C(1)); 90.4 ($^1J_{C,H}$ = 157.3, C(5) or C(15)); 95.7 ($^1J_{C,H}$ = 157.0, C(5) or C(15)); 159.8, 161.9, 162.9, 163.8, 168.0, 172.0, 173.6 (7 quart. sp^2–C). MS (120°): 602 (*100*, M^+), 601 (9), 587 (5), 586 (10), 572 (8), 571 (21), 557 (4), 556 (5), 542 (12), 541 (5). Anal. calc. for $C_{34}H_{51}CoN_6$ (602.8): C 67.75, H 8.53, N 13.94; found: C 67.27, H 8.46, N 13.94.

A compound showing the same anal. data as described was obtained when $NaBD_4$ was used instead of $NaBH_4$ as reducing agent in EtOH.

Electrosynthesis of **1**. In a conventional H-type electrochemical cell, 10 ml of 0.1M $LiClO_4$ in MeOH was preelectrolyzed at – 1.8 V *vs.* Ag/0.01M $AgNO_3$ in MeOH. The working electrode consisted of a stirred mercury pool (11 cm^2). When the residual current dropped below 100 μA, 389 mg (0.5 mmol) of dibromo[1-hydroxy-8H-HDP]cobalt(III) **2a** was added to the cathodic compartment. During electrolysis at – 1.8 V, the brown solution turned greenish. After 4 h, the current dropped to a constant value (1 mA), dark-green crystals precipitated, and coulometry showed 256 C corresponding to 4F electrons exchanged per mol of **2a** (with background current correction). The crystals were filtered off under Ar, washed with H_2O (3 × 10 ml), and dried at r.t. (48 h, 0.01 Torr): 242 mg (80.3%) of **1**. IR, ^{1}H-NMR, and MS of these crystals were superimposable to those of **1** obtained by $NaBH_4$ reduction.

[1-(D)Hydro-8H-HDP]cobalt(I) (D)-**1**. In the same manner as described above, 134 mg (0.2 mmol) of **2b** was reduced using $NaBH_4$ in EtOD or $NaBD_4$ in EtOD leading to (D)-**1** in yields of 66 or 53%, resp. IR: 2970, 1725, 1375, 1130. ^{1}H-NMR: 0.92–1.46 (48H, 16 CH_3 resolved in 8 lines at 0.92, 1.00, 1.13, 1.16, 1.27, 1.33, 1.39, 1.46); 5.31 (*s*, 1H, H–C(5) or H–C(15)); 5.44 (*s*, 1H, H–C(5) or H–C(15)). MS (100°): 603 (*100*, M^+), 602 (27), 601 (8), 588 (7), 587 (5), 586 (5), 573 (17), 572 (6), 571 (3), 558 (3), 557 (2), 543 (11), 542 (4), 541 (3).

REFERENCES

[1] *R. Scheffold & R. Orlinski*, J. Am. Chem. Soc. *105*, 7200 (1983).
[2] *R. Scheffold, J. Löliger, H.-U. Blaser & P. Geisser*, Helv. Chim. Acta *58*, 49 (1975).
[3] Review: *R. Scheffold, G. Rytz & L. Walder*, 'Modern Synthetic Methods', Vol. 3, ed. R. Scheffold, Salle, Frankfurt, Sauerländer, Aarau, Wiley, New York, 1983, pp. 355–440.
[4] Review: *K.L. Brown*, in 'B_{12}', Vol. 1, ed. D. Dolphin, Wiley, New York, 1982, pp. 245–294.
[5] *J.D. Brodie & M. Poe*, Biochemistry *10*, 914 (1971).
[6] *G.H. Beaven & E.A. Johnson*, Nature (London) *176*, 1264 (1955).
[7] a) *P.K. Das, H.A.O. Mill, J.M. Pratt & R.J.P. Williams*, Biochim. Biophys. Acta *141*, 644 (1967); b) *S.M. Chemaly & J.M. Pratt*, J. Chem. Soc., Dalton Trans. *1984*, 595.
[8] *D. Lexa & J.M. Savéant*, J. Chem. Soc., Chem. Commun. *1975*, 872.
[9] *D. Lexa, J.M. Savéant & J. Zickler*, J. Am. Chem. Soc. *99*, 2786 (1977).
[10] *D. Lexa & J.M. Savéant*, J. Am. Chem. Soc. *98*, 2652 (1976).
[11] *H.W. Whitlock & B.K. Bower*, Tetrahedron Lett. *1965*, 4827.
[12] *H. Kobayashi, T. Hara & Y. Kaizu*, Bull. Chem. Soc. Jpn. *45*, 2148 (1972).
[13] *D.H. Busch, J.H. Weber, D.H. Williams & N.J. Rose*, J. Am. Chem. Soc. *86*, 5161 (1964).
[14] *G.N. Schrauzer & R.J. Holland*, J. Am. Chem. Soc. *93*, 1505 (1971).
[15] *M. Naumberg, K.N.V. Duong & A. Gaudemer*, J. Organomet. Chem. *25*, 231 (1970).
[16] *R. Schwesinger, R. Waditschatka, J. Rigby, R. Nordmann, W.B. Schweizer, E. Zass & A. Eschenmoser*, Helv. Chim. Acta *65*, 600 (1982) and lit. cit. therein.
[17] *G. Rytz & R. Scheffold*, Helv. Chim. Acta *63*, 733 (1980).
[18] *L. Walder, G. Rytz, K. Meier & R. Scheffold*, Helv. Chim. Acta *61*, 3013 (1978).
[19] *R. Scheffold & E. Amble*, Angew. Chem. *92*, 643 (1980); Int. Ed. *19*, 629 (1980).
[20] *R. Scheffold, M. Dike, S. Dike, T. Herold & L. Walder*, J. Am. Chem. Soc. *102*, 3642 (1980).
[21] *R. Scheffold, G. Rytz, L. Walder, R. Orlinski & Z. Chilmonczyk*, Pure Appl. Chem. *55*, 1791 (1983).
[22] *W.C. Hamilton, J.S. Rollett & R.A. Sparks*, Acta Crystallogr. *18*, 129 (1965).
[23] *M.J. Buerger*, 'Vector Space', Wiley, New York, 1959.
[24] *J.A. Ibers & W.C. Hamilton*, 'International Tables for X-Ray Crystrallography', Vol. IV, The Kynoch Press, Birmingham, 1974.
[25] *P. Engel*, Acta Crystallogr., Sect. A *34*, 348 (1978).
[26] *J.P. Glusker*, in 'B_{12}', Vol. 1, ed. D. Dolphin, Wiley, New York, 1982, pp. 23–106.
[27] *U. Vogel*, Ph. D. Thesis, University of Bern, 1975.
[28] *H.C. Mez, J. Löliger, U. Vogel, K. Meier & R. Scheffold*, Helv. Chim. Acta *64*, 1098 (1981).
[29] *K. Meier, R. Scheffold & P. Engel*, Helv. Chim. Acta *64*, 1496 (1981).
[30] *W. Stegman, P. Gilgen, W. Heimgartner & H. Schmid*, Helv. Chim. Acta *59*, 1018 (1976).
[31] *D.F. Ewing*, in 'Annual Reports on NMR-Spectroscopy', Vol. 6A, ed. E.F. Mooney, Academic Press, New York, 1975, p. 389.
[32] *U. Vögeli, D. Herz & W. von Philipsborn*, Org. Magn. Reson. *13*, 200 (1980).
[33] *K.M. Kadish, L.A. Bottomley & D. Berioz*, Inorg. Chem. *17*, 1124 (1978).
[34] *L.A. Truxillo & D.G. Davis*, Anal. Chem. *47*, 2260 (1975).
[35] *V. Gutmann & E. Wychera*, Inorg. Nucl. Chem. Lett. *2*, 257 (1966).
[36] *K.R. Ashley & J.G. Leipoldt*, Inorg. Chem. *20*, 2326 (1981).
[37] *J.F. Endicott, J. Lilie, J.M. Kuszaj, B.S. Ramaswamy, W.G. Schmonsees, M.G. Simic, M.D. Glick & D.P. Rillema*, J. Am. Chem. Soc. *99*, 429 (1977).
[38] *V.L. Goedken & S.M. Pen*, J. Chem. Soc., Chem. Commun. *1974*, 914.
[39] *N. Takvoryan, K. Farmery, V. Katovic, F.V. Lovecchio, E.S. Gore, L.B. Anderson & D.H. Busch*, J. Am. Chem. Soc. *96*, 731 (1974).
[40] *N.S. Hush & I.S. Woolsey*, J. Am. Chem. Soc. *94*, 4107 (1972).
[41] *B. Kräutler & K. Hilpert*, Angew. Chem. Suppl. *1982*, 305–316.
[42] *D.F. Shriver*, 'The Manipulation of Air Sensitive Compounds', Mc Graw-Hill, New York, 1969.